
Structural Design and Optimization of Nonuniform Chiral Phononic Crystals for Vehicle Interior Noise Reduction

Tao Yuan, Hui Guo, Yansong Wang, Pei Sun and Yi Wang

School of Mechanical and Automotive Engineering, Shanghai University of Engineering Science, Shanghai, China.
E-mail: hgsues@163.com

(Received 27 November 2022; accepted 3 April 2023)

Phononic crystals (PnCs) with nonuniform and chiral design are developed and applied for the reduction of vehicle interior noise. To investigate the effects of structural parameters such as the lattice arrangements and the filling rates, locally resonant PnCs (LRPnCs) are established for calculating sound insulation and bandgap characteristics. Furthermore, the nonuniform LRPnCs with Greek-cross chiral structure are constructed. To improve the sound insulation characteristics of the nonuniform chiral LRPnCs, a genetic algorithm (GA) optimization procedure is performed. Accordingly, the modified nonuniform chiral LRPnCs is designed and simulated to predict the sound insulation characteristics. Experimental verification suggests that the simulated results are in good agreement with the tested ones. The newly designed nonuniform chiral LRPnCs are effective in vehicle interior noise reduction. All the works are expected to be extended to other sound-related fields for noise reductions in engineering.

1. INTRODUCTION

There has been an increasing interest in vehicle interior noise in recent years, and mainly two approaches exist for suppressing interior noise in vehicle engineering: active noise control (ANC) and passive noise control (PNC).^{1,2} Compared to ANC which based on the superposition principle of sound waves, PNC depends on the design of vehicle sound packages, and due to the large sound wavelength, it is difficult to extend the effectively controlled frequency range of PNC to low frequencies. Therefore, functional materials and structures are introduced into the field of vehicle noise control.^{3,4} Among them, the phononic crystals (PnCs) with good sound insulation and bandgap characteristics, which could be used to selectively suppress elastic waves by a small-size structure, have been receiving more attention.

According to the formation mechanism of bandgaps, the PnCs are divided into two catalogs, the Bragg scattering PnCs (BSPnCs)⁵ and the locally resonant PnCs (LRPnCs).⁶ Since the spatial modulations of bandgap have the same orders of magnitude as the wavelengths, the size of a BSPnCs for eliminating the low-frequency noises will be extremely large.^{7,8} Due to the insufficient layout spaces in the vehicles, the BSPnCs are not suitable for reducing the low-frequency vehicle noises. While the LRPnCs block sound wave propagations by oscillator resonances occurred in a frequency range corresponding to the wavelengths far less than the lattice scale and overcoming the low-frequency defects of the BSPnCs.^{9,10} Various LRPnCs structures are developed and LRPnCs plates with cylindrical stubs have received considerable attention. Pennec et al.¹¹ design a LRPnCs plate constituted of a periodical array of cylindrical stubs deposited on a thin plate, and theoretically find that the opening of the bandgap depends on the geometrical parameters. A similar conclusion is obtained in the works by Wu et al.,¹² which a LRPnCs plate with periodic cylinder stubbed surface is numerically and experimentally studied. Oudich et al.¹³ study a LRPnCs plate with cylin-

dric stubs experimentally and the stubs play a key role in the structure behavior. The above cylindrical stubs are made of homogeneous material, while cylindrical stubs with different materials are also investigated.^{14,15} In addition, more forms of LRPnCs plates, such as square stubs structures and no-stubs plates are proposed. Multiple square stubs LRPnCs plates are investigated by Wang et al.¹⁶ and the LRPnCs have wide bandgaps at lower frequencies comparing with one stub structure. Zhou et al.¹⁷ report a multilayered LRPnCs plates with coaxial rubber and metal shells and point out that the bandgap frequencies can be adjusted by the design of the multilayered structure. The aforementioned research suggests that LRPnCs plates have good bandgap characteristics in low-frequency ranges, and comparing with the plates with stubs, the no-stubs LRPnCs plates have relatively small thickness and are more suitable for interior noise control of vehicles. In addition, chiral topologies are introduced to the design of PnCs because of the unique mechanical properties such as high shear rigidity and negative Poisson's ratio.¹⁸ Spadoni et al.¹⁹ report a PnCs plate with hexagonal chiral lattices, and the bandgap occurrence are related to the ratios of two lattices. Chen et al.²⁰ obtained the complete bandgap of a hexachiral PnCs plate by optimization method. The chiral design provides new perspectives for the controlling of the bandgap properties of PnCs.

Based on the above findings, it is feasible to reduce the low-frequency noises in vehicle interior by the using of the PnCs plates. The previous studies are mainly focused on uniformly arranged PnCs plates. Taking the chiral design into consideration, it can be assumed that the introduction of nonuniformly arranged PnCs plates with chiral topologies might be a new way to reduce the vehicle interior noise in some specific frequency bands. Therefore, based on the bandgap characteristics, this paper presents a new type of nonuniform chiral LRPnCs, and discusses the effects of the structural parameters on the sound insulation characteristics in different frequency bands. Aiming at the interior noise reduction at different frequencies, the chiral units are applied in the nonuniform chiral

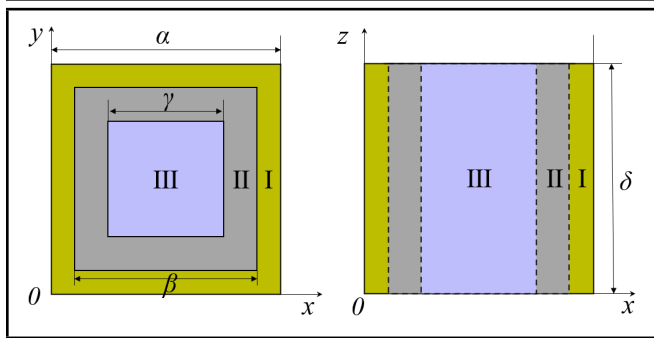


Figure 1. Designed structure of the lattice of the LRPnCs.

Table 1. The property parameters of materials in PnCs unit.

Materials	Layers	$\rho(\text{kg}\cdot\text{m}^{-3})$	$E(\text{Pa})$	ν
Epoxy resin	I	1180	0.43×10^{10}	0.16
EPDM	II	1400	1.17×10^5	0.47
Steel	III	7760	21.07×10^{10}	0.30

LRPnCs for optimization design. Simulations and experiments are conducted to verify the effectiveness of the nonuniform chiral LRPnCs.

2. DESIGN AND SOUND INSULATION ANALYSIS OF NONUNIFORM LRPnCS

A unit structure (lattice) of LRPnCs with three components is designed in Fig. 1, in which the substrate (outer layer I) was epoxy resin, the connector (middle layer II) was ethylene propylene diene monomer (EPDM), and the scatterer (vibrator) (inner body III) was set as steel. The dimension parameters of the lattice were $\alpha=20\text{mm}$, $\beta=16\text{mm}$, $\gamma=10\text{mm}$ and $\delta=20\text{mm}$, the cross-sections of I, II and III were squares. The related property parameters of materials are listed in Table 1, where ρ is density, E the Young's modulus and ν the Poisson's ratio.

The sound insulation and bandgap characteristics of the LRPnCs can be obtained from the Finite Element Method (FEM). The governing equations of an elastic wave in an ideal medium can be simplified as:

$$\rho\omega^2\mathbf{u}(\mathbf{r}) + (\lambda + \mu)\nabla(\nabla \cdot \mathbf{u}(\mathbf{r})) + \mu\nabla^2\mathbf{u}(\mathbf{r}) = 0; \quad (1)$$

where, μ and λ are the Lamé constants, ∇ is the Hamilton differential operator. $\mathbf{u}(\mathbf{r})$ is the displacement, \mathbf{r} is the position vector, ω is the angular frequency of the elastic wave. According to the Bloch's theorem,²¹ when a sound wave propagates through a periodic structural medium, its displacement field can be described as:

$$\mathbf{u}(\mathbf{r}) = e^{i(\mathbf{k}\cdot\mathbf{r})}\mathbf{u}_{\mathbf{k}}(\mathbf{r}); \quad (2)$$

where, \mathbf{k} is the Bloch wave vector. In the FEM modeling, the eigenvalue equation in discrete form can be established as:

$$(\mathbf{K} - \omega^2\mathbf{M})\mathbf{U} = 0; \quad (3)$$

where, \mathbf{K} and \mathbf{M} are the stiffness and mass matrices, \mathbf{U} is the displacement at nodes. Taking the LRPnCs as an example, the exterior boundary condition of the unit satisfies:

$$\mathbf{U}(\mathbf{r}+\mathbf{a}) = e^{i(\mathbf{k}\cdot\mathbf{a})}\mathbf{U}(\mathbf{r}); \quad (4)$$

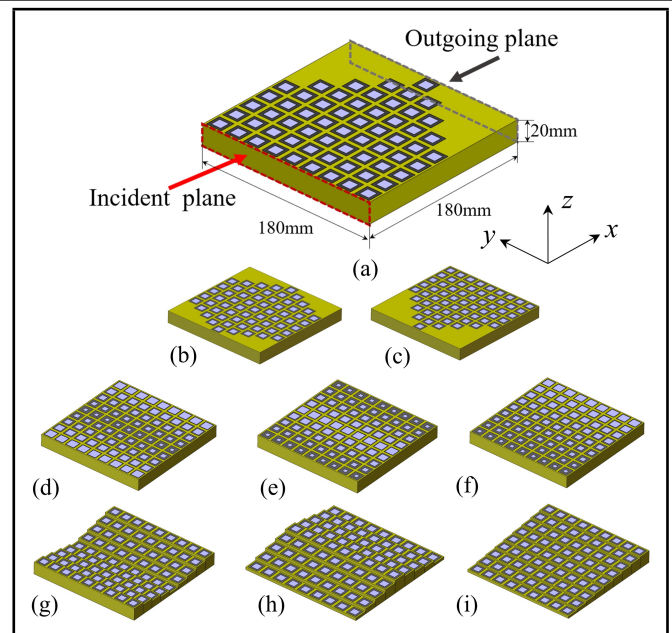


Figure 2. The designed nonuniform LRPnCs with different structures.

where, \mathbf{a} is the lattice base vector. In this paper, COMSOL is used to solve the eigenvalue Eq. (3) under the exterior boundary condition of Eq. (4). A complete band structure can be obtained by sequentially taking the values of \mathbf{k} from the reduced Brillouin scattering area.

To study the effects of structural parameters on sound insulation characteristics of the nonuniform LRPnCs, we designed nine nonuniform LRPnCs models with different lattice arrangements, filling rates and substrate thicknesses (vibrator lengths), while the vibrator materials were steel. The over-size of all nine models was $180\text{mm} \times 180\text{mm} \times 20\text{mm}$. The transmission losses of the models are simulated via COMSOL. The sound incident and outgoing planes of all models have the same configurations with model (a), the left side faces are the incident planes, and the opposite ones are the outgoing planes, as shown in Fig. 2. The vibrators of model (a) and model (c) were arranged near the sound incident and outgoing planes, while the vibrators of model (b) were arranged around the geometric center of the plate. In the models (d) and (e), the vibrator filling rates were set to increase and decrease from middle row to both the sound incident and outgoing ends respectively, and the filling rate of model (f) increases from the incident end to the outgoing end. The vibrator lengths of models (g) and (h) increased and decreased from the middle row to both the sound incident and outgoing ends respectively, and the vibrator lengths of model (i) increased from the incident end to the outgoing end. If an incident noise passes through the lattice surface, the structural sound transmission loss may be defined as:

$$TL = 10\log E_i - 10\log E_t = 10\log \left(\frac{E_i}{E_t} \right); \quad (5)$$

where, TL was the sound transmission loss (in dB), E_i and E_t were the incident and the transmitted sound energies. The sound transmission loss of the nine nonuniform LRPnCs are displayed in Fig. 3, Fig. 4 and Fig. 5.

The calculated sound transmission losses of the models (a), (b) and (c) are compared in Fig. 3. Regardless of the lattice arrangements, there were three transmission loss peaks in the

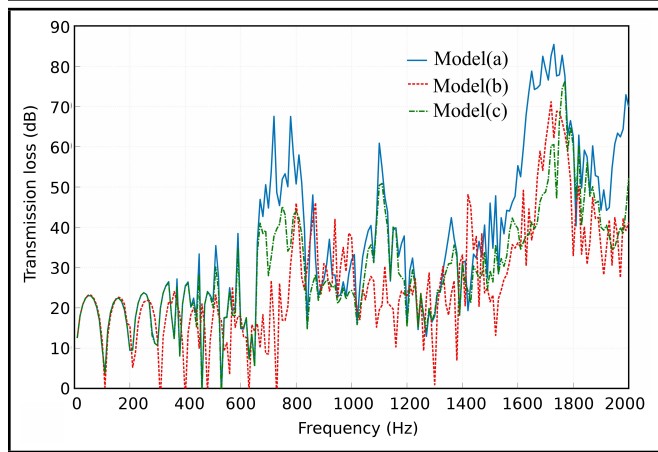


Figure 3. Sound transmission losses of models (a), (b) and (c) with different lattice arrangements.

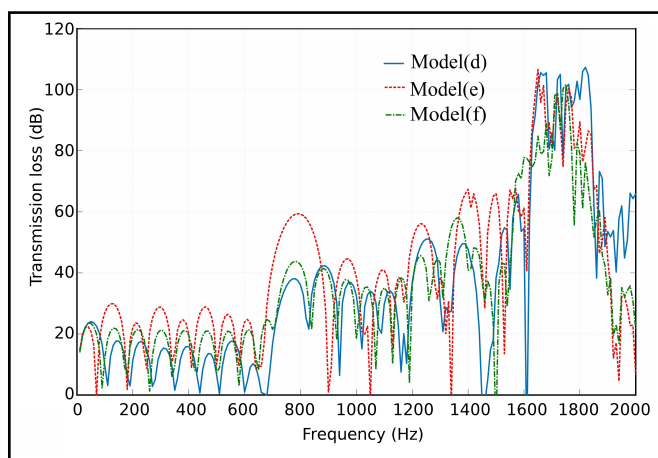


Figure 4. Sound transmission losses of models (d), (e) and (f) with different filling rates.

frequency range from 650Hz to 1850Hz. The model (a) obtained the best sound insulation results in the whole frequency range, especially in the bands [650, 850] Hz, [1050, 1200] Hz and [1600, 1800] Hz, and its maximum transmission loss reached 85dB. Compared with model (a), the transmission loss peaks of model (b) slightly move towards higher frequencies, and model (c) has similar peak frequencies, but the sound insulation performance was obviously weakened. It can be concluded that the closer the lattices were arranged to the incident sound plane, the better the sound insulation performance in a lower frequency range. The sound insulation characteristics of the nonuniform LRPnCs with different filling rates were depicted in Fig. 4. In comparison of the sound insulation performance, model (e) was the best. The maximum differences between the transmission loss peaks of model (e) and model (d) were 15dB at 480Hz and 25dB at 790Hz. In the higher frequency range above 1600Hz, the transmission losses of model (d) were slightly larger than those of model (e). In view of the model thicknesses, the sound insulation performances of the models (g), (h) and (i) shown in Fig. 5 have a little difference. However, the sound insulation performance of the model (g) was the best at the low frequencies less than 600Hz, and the transmission losses of the model (h) with a maximum 95 dB were larger at the middle and high frequencies. This implies that the sound insulation requirements of different frequency bands can be met by changing the thickness distribution of

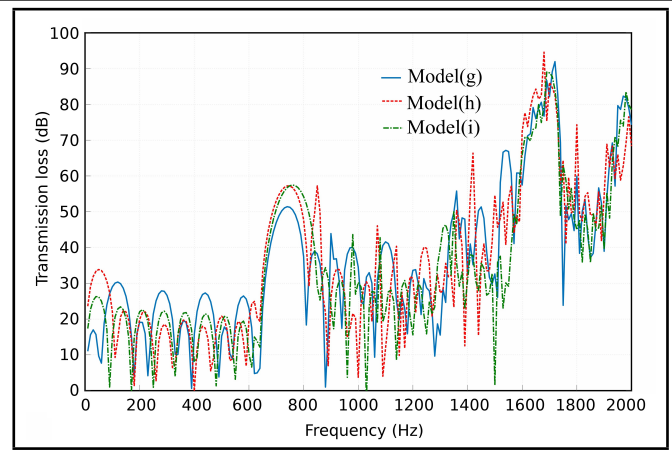


Figure 5. Sound transmission losses of models (g), (h) and (i) with different thicknesses.

PnCs. Because of model thickness on the surface localized modes, there were some local bandgaps in the frequency range [900, 1400] Hz, which may be the results of complex couplings among the torsional modes of the models.

Based on the above analysis, it can be found that the sound insulation performance of the nonuniform LRPnCs is depended on the structural designs, model (a) with steel vibrator shows relatively better sound insulation performance.

3. STRUCTURAL DESIGN AND OPTIMIZATION OF NONUNIFORM CHIRAL LRPnCS

Previous studies suggest that the using of the chiral structure is an effective way to design a new kind of PnCs. Considering the low-frequency and wide-band wave absorbing characteristics of the chiral structure, the Greek-cross chiral design was introduced to the nonuniform LRPnCs in this paper.

3.1. Design and Simulation of Nonuniform Chiral LRPnCs

Taking the sound transmission losses, the manufacturing feasibility, and the cost of the samples into consideration, model (a) in Fig. 2 is selected as an example, the Greek-cross chiral units were used to substitute the cube steel vibrator for studying the energy-band structure of PnCs. The structure of the chiral unit is shown in Fig. 6, and the structural parameters b , c , d , e and f satisfy: $f=16\text{mm}$, $b < f$, $d=0.5 \times (b-c)$, $e=d-c$. The material of Greek-cross vibrator was steel, and the material properties of other components are the same as those in Table 1.

To study the effects of Greek-cross structural parameters b and c on sound insulation characteristics, firstly, setting $c=0.1f$ and b increased from $0.6f$ to $0.9f$, the calculated transmission losses of some models are shown in Fig. 7. In the frequency range below 1500Hz, the transmission losses of the nonuniform chiral LRPnCs increased with the increase of b , the peak value of transmission loss increases from 68dB to 130dB, and the main sound insulation band extends from [1390, 1440] Hz to [1180, 1510] Hz. An opposite conclusion may be drawn in the frequency range above 1500Hz. A larger b value was beneficial to generate a wider bandgap at the middle and low frequencies. The reason was that an increased b lead to a de-

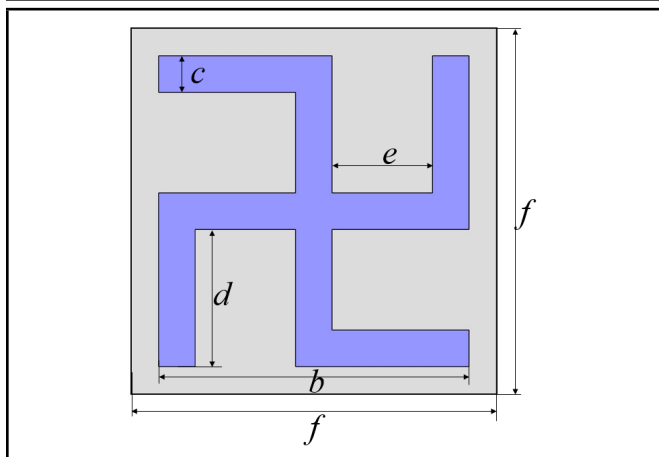


Figure 6. The Greek-cross chiral units.

creased stiffness of chiral vibrator and enhances energy localization ability at the lower frequencies.

Furthermore, under the conditions $b=0.9f$ and c increased from $0.1f$ to $0.25f$, the transmission losses of the nonuniform chiral LRPnCs models are also calculated, as shown in Fig. 8. With the increase of c , the peak value of transmission loss increased slightly at first and then decreased, the main frequency band of sound insulation shrunk from [1180, 1510] Hz to [1540, 1660] Hz and moved to the high frequency direction. The results suggest that a properly selected c is helpful for the increase of transmission loss in the middle and low frequency ranges.

From the above analysis a conclusion can be drawn that the transmission losses of the nonuniform chiral LRPnCs were dependent on the structural parameters. Since the materials of the vibrators are set as steel, proper structure design of the nonuniform chiral LRPnCs could lead to a satisfied sound insulation performance. Furthermore, there are mainly two frequency bands under 1500Hz for a certain nonuniform chiral LRPnCs, as illustrated in Fig. 7 and Fig. 8, and the second band has the highest transmission loss.

3.2. Structural Optimization of the Nonuniform Chiral LRPnCs for Vehicle Noise Reduction

In this work, the nonuniform chiral LRPnCs was adopted for selectively reducing the interior noise of a family vehicle. Under a constant speed 100 km/h, the ear-side noises of passengers were collected, and thereby their frequency spectra were calculated, the vehicle interior noise was mainly concentrated in the frequency bands [100, 400] Hz and [900, 1150] Hz. According to the foregoing study results, in term of the noise reduction, the nonuniform chiral LRPnCs were more sensitive to the second frequency band. Thus, aiming at noise reduction in [900, 1150] Hz, the genetic algorithm (GA) was selected and used to optimize the structural parameters of the nonuniform chiral LRPnCs model.

As an optimal solution searching method, the GA has been widely used in the fields of machine learning, data mining, image processing, etc. The operation process of GA includes parameter coding, initial population selection, fitness function definition, control parameter selection and genetic operation setting, etc. We selected b and c as the structural parameters to be optimized and initially sets $b=[0.6f, 0.9f]$ with an interval

$0.02f$ and $c=[0.04f, 0.19f]$ with an interval $0.01f$. Combining the values of b and c randomly, 256 models can be obtained. The TL of each model can be obtained by COMSOL simulation. The total value of TL of each model within the frequency band [900, 1150] Hz were calculated. Summarizing the result data into matrix form, a matrix $[b, c, TL]$ with a dimension of 256×3 was established. A function of TL about the parameters b and c can be finally obtained by data fitting. In this paper, the 1stOpt-based fitting method and the MATLAB-based polynomial fitting method were applied. As for the fitting errors of the two methods, the root mean square error (RMSE) of the MATLAB-based fitting method is 0.81, while the 1stOpt-based fitting method is 1.75. Then the MATLAB-based polynomial fitting method was better and used for the structural optimization, the fitted surface is shown in Fig. 9. The corresponding fitness function is established as:

$$\begin{aligned}
 TL = & p_{00} + p_{10}b + p_{01}c + p_{20}b^2 + p_{11}bc \\
 & + p_{02}c^2 + p_{30}b^3 + p_{21}b^2c \\
 & + p_{12}bc^2 + p_{03}c^3 + p_{40}b^4 \\
 & + p_{31}b^3c + p_{22}b^2c^2 + p_{13}bc^3 \\
 & + p_{04}c^4 + p_{41}b^4c + p_{32}b^3c^2 \\
 & + p_{23}b^2c^3 + p_{14}bc^4 + p_{05}b^5
 \end{aligned} \quad ; \quad (6)$$

where, $p_{00}=-3003.000$, $p_{10}=1095.000$, $p_{01}=1006.000$, $p_{20}=-147.200$, $p_{11}=-408.500$, $p_{02}=192.500$, $p_{30}=8.682$, $p_{21}=61.730$, $p_{12}=-58.510$, $p_{03}=20.310$, $p_{40}=-0.190$, $p_{31}=-3.998$, $p_{22}=4.527$, $p_{13}=2.831$, $p_{04}=-10.720$, $p_{41}=0.095$, $p_{32}=-0.103$, $p_{23}=-0.298$, $p_{14}=0.793$ and $p_{05}=0.013$.

After 51 iterations, the optimal solutions were $b=14.400\text{mm}$, $c=1.386\text{mm}$, $f=16\text{mm}$ ($b=0.9f$, $c=0.0866f$), and the TL was 39.43dB, while the TL of original design with $b=0.85f$, $c=0.1f$ was 24dB, and the optimal sound insulation property of PnCs was reached and with an increasing of 15.43dB in TL . The nonuniform chiral LRPnCs with Greek-cross are demonstrated in Fig. 10, and the overall size is $180\text{mm} \times 180\text{mm} \times 5\text{mm}$.

4. EXPERIMENTAL VERIFICATION FOR VEHICLE INTERIOR NOISE REDUCTION

To verify the simulation and optimization results, a sample of the optimized nonuniform chiral LRPnCs was made and shown in Fig. 11. The sample was put into a vehicle cavity model for measuring noise reduction, the cavity had an overall size of $650\text{mm} \times 650\text{mm} \times 400\text{mm}$ and was made of acrylic plates. The testing equipment, including a 40-channel LMS data acquisition system, three PCB microphones, a volume sound source, and a power amplifier, etc., were set as those in Fig. 12. During the tests, the incident sound wave was an amplified white noise in a frequency range from 50Hz to 2048Hz. The microphone collected the sound pressure signal of each measuring point through the LMS system, and the sampling frequency was set to 6.4 kHz. The tests were carried out in a semi-anechoic chamber with a background noise lower than 18dB.

To verify the simulated result, the sound transmission loss of the nonuniform chiral LRPnCs sample was tested, as illustrated in Fig. 12(b). To ensure that the incident sound was plane wave, the sample was horizontally placed inside a closed fixture (the folder), and the conical head of the sound source was placed in front of the sample with a distance of 15cm. Two microphones were respectively installed at 3cm away from the

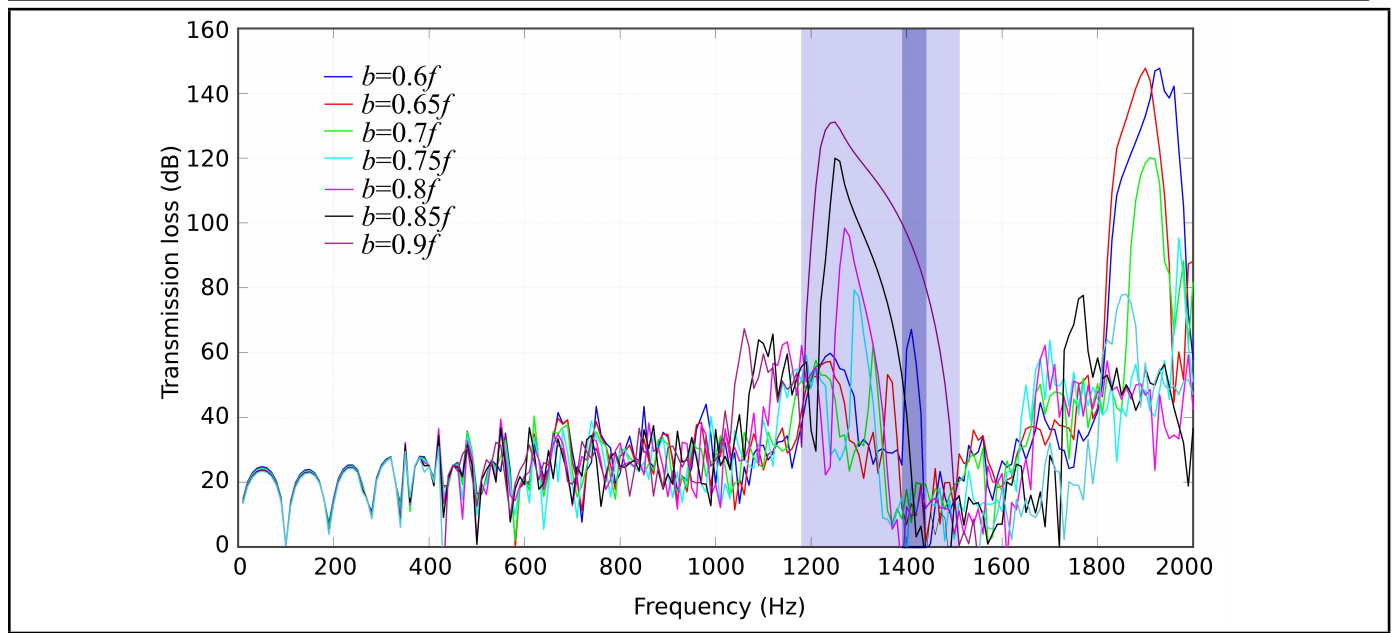


Figure 7. Transmission losses of the nonuniform chiral LRPnCs with different b values.

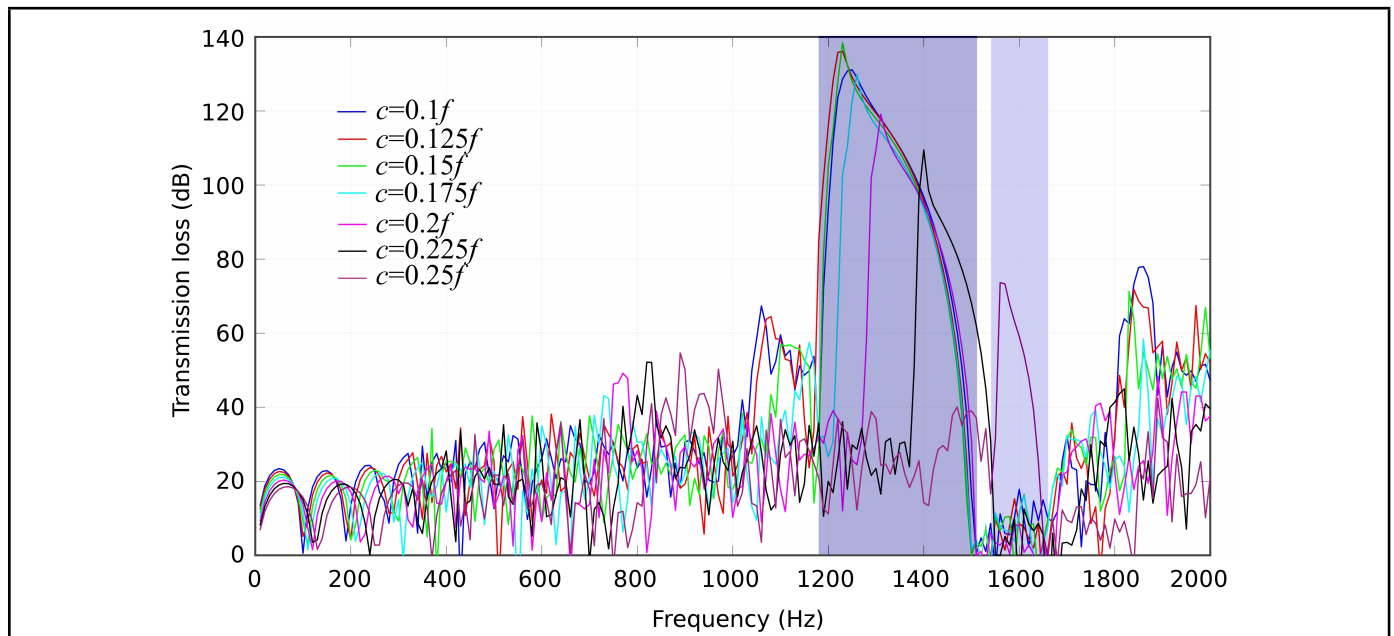


Figure 8. Transmission losses of the nonuniform chiral LRPnCs with different c values.

front and back ends of the sample to collect the incident and outgoing sound pressures. The simulated and tested transmission losses of the sample are compared in Fig. 13. The changing patterns of TL obtained from the simulation and test are the same, the maximum TL are 74dB at 1192Hz in simulation, and 76dB at 1074Hz in experiment, respectively. This suggests that the calculation results of finite element simulation are effective.

After testing the sound insulation characteristics, the noise reduction test was carried out by replacing the closed fixture with the cavity model containing the sample, as shown in Fig.12(a) and 12(c). The nonuniform chiral LRPnCs were pasted on the top inside of the cavity model, the sound source was placed at 200mm away from the front panel of the cavity, and the microphone was fixed at a virtual driver’s ear-side position (330mm, 180mm, 400mm) in the cavity model to measure

sound pressure signal. The sound pressure levels (SPLs) at the driver’s ear side in the cavity model measured under the conditions of with and without the nonuniform chiral LRPnCs are compared in Fig. 14. After the adding of the nonuniform chiral LRPnCs, the peak values of SPL at 975Hz, 1038Hz, 1087Hz and 1146Hz decreased by 2dB to 4dB, which suggests the effectiveness and reasonableness to use the nonuniform chiral LRPnCs for reducing the vehicle interior noise in a specific frequency band.

It should be mentioned that, although the simulated and experimental measured results are basically consistent in Fig. 13, there still have some differences in the amplitudes of transmission loss, which might be caused by the sample manufacturing errors and/or the boundary condition differences in the experiment and simulation settings.

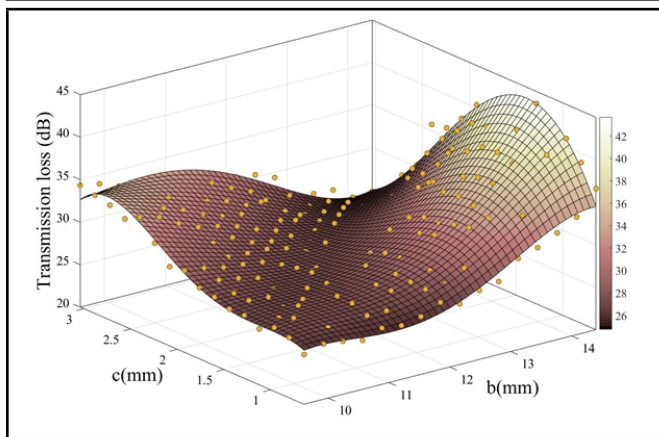


Figure 9. The result of MATLAB-based polynomial fitting method.

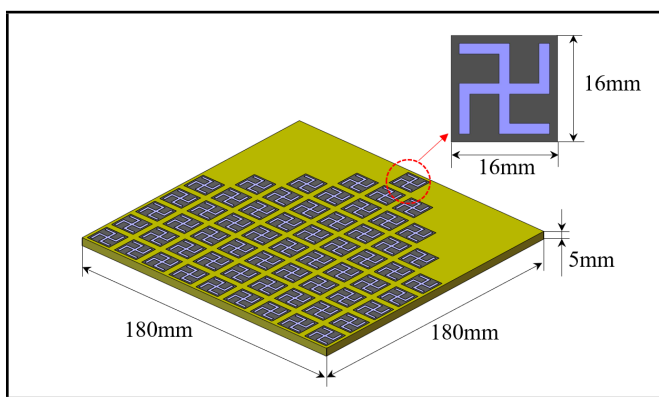


Figure 10. The optimized nonuniform chiral LRPnCs.

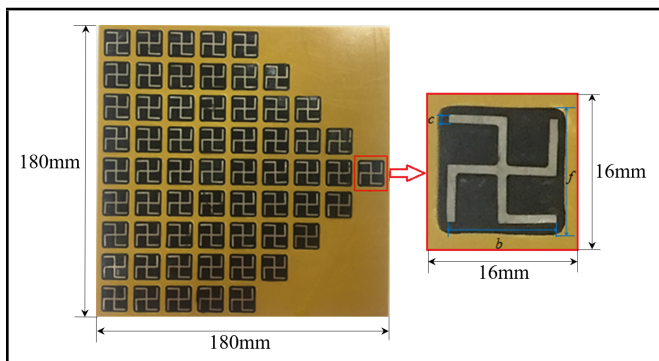


Figure 11. A testing sample of the nonuniform chiral LRPnCs with optimized parameters.

5. CONCLUSIONS

This paper presents nonuniform chiral locally resonant phononic crystals (LRPnCs) for the noise reduction in vehicles. The effects of lattice arrangements, filling rates and vibrator thicknesses on the sound insulation characteristics of the PnCs are studied. The Greek-cross vibrators are introduced to study the sound insulation characteristics of the PnCs. The structural parameters of a chiral vibrator are optimized by using GA for reducing the interior noise in certain frequency range. The simulated results are verified by experimental data. The results show that the closer the vibrators arranged to the incident sound plane, the greater the transmission loss of the nonuniform chiral LRPnCs is, and the sound-insulation frequency band moves to the low-frequency direction. The distribution of the vibrator filling rate, which has a great influence

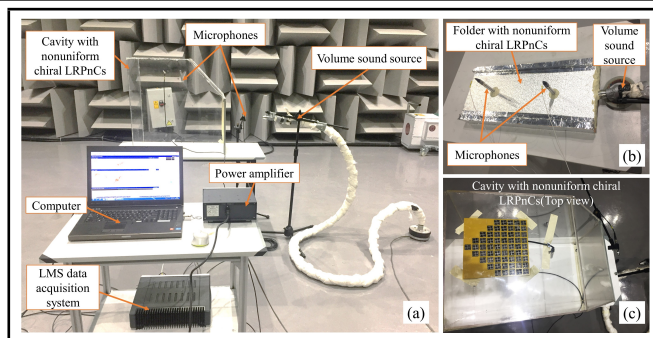


Figure 12. Experimental settings for measurements of transmission loss and interior noise reduction: (a) measurement system, (b) transmission loss test settings, (c) cavity with nonuniform chiral LRPnCs for interior noise reduction.

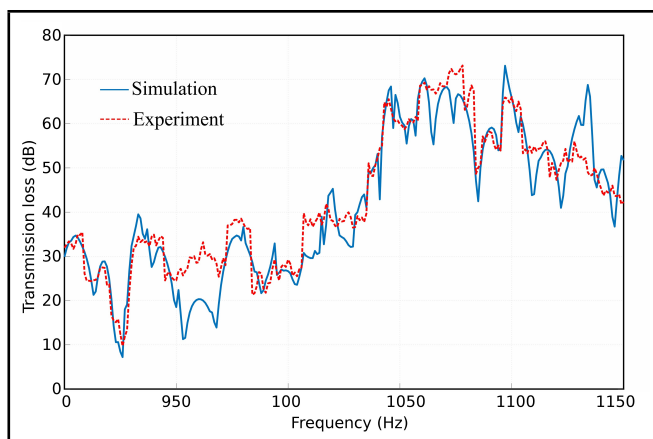


Figure 13. Comparison of the simulated and measured TL s of the LRPnCs.

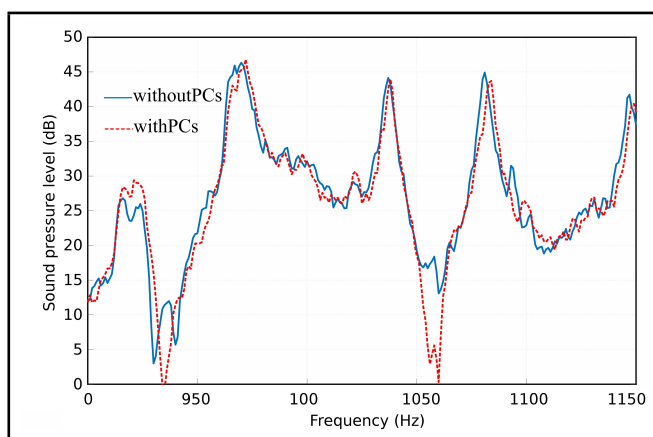


Figure 14. Comparison of SPLs with and without LRPnCs in interior cavity.

on the sound insulation characteristics at low frequencies, may cause local attenuation in sound insulation ability. The substrate thickness distribution can be adjusted to meet the sound insulation requirements of different frequency bands, and the nonuniform chiral LRPnCs with a thickness reduction from both sides to the middle is more suitable for low-frequency sound insulation. For the vehicle interior noise in the middle and low frequency range, the nonuniform chiral LRPnCs with chiral structural parameters $b=14.400\text{mm}$ and $c=1.386\text{mm}$ has an optimal sound insulation performance. The experimental verifications suggest that the simulated transmission losses are in good agreement with the tested ones, and the optimized nonuniform chiral LRPnCs is effective for reducing the vehicle

interior noise in a specified frequency band. In the future studies, smart materials such as piezoelectric materials might be introduced and structural parameters can be further optimized to make the sound insulation bandgaps of the PnCs develop towards the direction of low frequency and wide band, to achieve more effective noise reduction of vehicles.

ACKNOWLEDGEMENTS

This work was supported by the Project of National Natural Science Foundation of China (No.52005318, No.52172371), and partly sponsored by the Program for Shanghai Academic Research Leader (No. 21XD1401100) and the Project of Technical Service Platform for Noise and Vibration Evaluation and Control of New Energy Vehicles (No.18DZ2295900) at Science and Technology Commission of Shanghai Municipality, China.

REFERENCES

- ¹ Z. S. Liu, H. P. Lee, C. Lu. Passive and active interior noise control of box structures using the structural intensity method. *Applied Acoustics*, **67.2**, 112-134 (2006). <https://doi.org/10.1016/j.apacoust.2005.04.010>
- ² H. Guo, Y. S. Wang, N. N. Liu, R. P. Yu, X. T. Liu. Active interior noise control for rail vehicle using a variable step-size median-LMS algorithm. *Mechanical Systems and Signal Processing*, **109**, 15-26 (2018). <https://doi.org/10.1016/j.ymsp.2018.02.040>
- ³ N. Gao, Z. Zhang, J. Deng, X. Guo, B. Cheng, H. Hou. Acoustic metamaterials for noise reduction: a review. *Advanced Materials Technologies*, **7**, 2100698 (2022). <https://doi.org/10.1002/admt.202100698>
- ⁴ H. Guo, Y. S. Wang, C. Yang, X. L. Wang, N. N. Liu, Z. J. Xu. Vehicle interior noise active control based on piezoelectric ceramic materials and improved fuzzy control algorithm. *Applied Acoustics*, **150**, 216-226 (2019). <https://doi.org/10.1016/j.apacoust.2019.02.018>
- ⁵ M. M. Sigalas, E. N. Economou. Elastic and acoustic wave band structure. *Journal of Sound and Vibration*, **158** (2), 377-382 (1992). [https://doi.org/10.1016/0022-460X\(92\)90059-7](https://doi.org/10.1016/0022-460X(92)90059-7)
- ⁶ Z. Liu, X. Zhang, Y. Mao, Y. Y. Zhu, Z. Yang, C. T. Chan, P. Sheng. Locally resonant sonic materials. *Science*, **289**, 1734-1736 (2000). <https://doi.org/10.1126/science.289.5485.1734>
- ⁷ A.O. Krushynska, M. Miniaci, F. Bosia, N.M. Pugno. Coupling local resonance with Bragg band gaps in single-phase mechanical metamaterials. *Extreme Mechanics Letters*, **12**, 30-36. (2017) <https://doi.org/10.1016/j.eml.2016.10.004>
- ⁸ Z. Jia, Y. Chen, H. Yang, L. Wang. Designing phononic crystals with wide and robust band gaps. *Physical Review Applied*, **9**, 044021 (2018). <https://doi.org/10.1103/PhysRevApplied.9.044021>
- ⁹ D. Yu, J. Wen, H. Zhao, Y. Liu, X. Wen. Vibration reduction by using the idea of phononic crystals in a pipe-conveying fluid. *Journal of Sound and Vibration*, **318**, 193-205 (2008). <https://doi.org/10.1016/j.jsv.2008.04.009>
- ¹⁰ Z. Tan, X. Sun, M. Tian, H. Zhu, T. Song, X. Wen, X. Liu, Z. Liu. The mechanism of bandgap opening and merging in 2D spherical phononic crystals. *Physics Letters A*, **405**, 127432 (2021). <https://doi.org/10.1016/j.physleta.2021.127432>
- ¹¹ Y. Pennec, B. Djafari-Rouhani, H. Larabi, A. Akjouj, J. N. Gillet, J. O. Vasseur, G. Thabet. Phonon transport and waveguiding in a phononic crystal made up of cylindrical dots on a thin homogeneous plate. *Physical Review B*, **80**, 144302 (2009). <https://doi.org/10.1103/PhysRevB.80.144302>
- ¹² T. Wu, Z. Huang, T. Tsai, T. Wu. Evidence of complete band gap and resonances in a plate with periodic stubbed surface. *Applied Physics Letters*, **93**, 111902 (2008). <https://doi.org/10.1063/1.2970992>
- ¹³ M. Oudich, M. Senesi, M. Assouar, M. Ruzenne, J. Sun, B. Vincent, Z. Hou, T. Wu. Experimental evidence of locally resonant sonic band gap in two-dimensional phononic stubbed plates. *Physical Review B*, **84**, 165136 (2011). <https://doi.org/10.1103/PhysRevB.84.165136>
- ¹⁴ S. Li, Y. Dou, T. Chen, Z. Wan, Z. Guan. A novel metal-matrix phononic crystal with a low-frequency, broad and complete, locally-resonant band gap. *Modern Physics Letters B*, **32**(19), 1850221 (2018). <https://doi.org/10.1142/S0217984918502214>
- ¹⁵ Y. Xiang, M. Chen, D. Qian, Z. Shi. Influence mechanism of a new-style resonator on band gap of locally resonant phononic crystal double panel structure. *Crystals*, **12**, 609 (2022). <https://doi.org/10.3390/cryst12050609>
- ¹⁶ X. Wang, P. Jiang, T. Chen, J. Zhu. Tuning characteristic of band gap and waveguide in a multi-stub locally resonant phononic crystal plate. *AIP Advances*, **5**, 107141 (2015). <https://doi.org/10.1063/1.4935067>
- ¹⁷ X. Zhou, Y. Xu, Y. Liu, L. Lv, F. Peng, L. Wang. Extending and lowering band gaps by multilayered locally resonant phononic crystals. *Applied Acoustics*, **133**, 97-106 (2018). <https://doi.org/10.1016/j.apacoust.2017.12.012>
- ¹⁸ D. Prall, R. Lakes. Properties of a chiral honeycomb with a Poisson's ratio of -1 . *International Journal of Mechanical Sciences*, **39**(3), 305-314 (1997). [https://doi.org/10.1016/S0020-7403\(96\)00025-2](https://doi.org/10.1016/S0020-7403(96)00025-2)
- ¹⁹ A. Spadoni, M. Ruzzene, S. Gonella, F. Scarpa. Phononic properties of hexagonal chiral lattices. *Wave Motion*, **46**, 435-450 (2009). <https://doi.org/10.1016/j.wavemoti.2009.04.002>
- ²⁰ L. Chen, Y. Guo, H. Yi. Optimization study of bandgaps properties for two-dimensional chiral phononic crystals base on lightweight design. *Physics Letters A*, **388**, 127054 (2021). <https://doi.org/10.1016/j.physleta.2020.127054>
- ²¹ N. Gao, H. Hou, B. Cheng, R. Zhang. A hollow inclusion self-similarity phononic crystal with an ultra-low-frequency bandgap. *International Journal of Modern Physics B*, **31**, 1850005 (2017). <https://doi.org/10.1142/S0217979218500054>